Tellus (2003), 55A, 45–60
Printed in UK. All rights reserved

TELLUS
ISSN 0280–6495

Large-scale waves interacting with deep convection in idealized mesoscale model simulations

By ADAM H. SOBEL[1*] and CHRISTOPHER S. BRETHERTON[2], [1]*Department of Applied Physics and Applied Mathematics, and Department of Earth and Environmental Sciences, Columbia University, New York, NY, USA;* [2]*Department of Atmospheric Sciences, University of Washington, Seattle, WA, USA*

(Manuscript received 2 January 2002; in final form 3 June 2002)

ABSTRACT

The authors study the interaction of large-scale waves with deep convection in nonrotating mesoscale model simulations, without mean vertical shear, under idealized boundary conditions (doubly periodic, fixed uniform sea surface temperature). Radiative cooling is fixed, so radiative–convective feedbacks are not considered. The model is initialized with random thermal perturbations near the surface and then run for 16 days to a state of approximate radiative-convective equilibrium. At this point, a wave-like heating is imposed for one day in order to create a wave. The heating is uniform in the meridional direction, sinusoidal with a wavelength equal to the domain size (4500 km) in the zonal direction, and has a roughly "first baroclinic mode" structure in the vertical. After this single day of forcing, the heating is turned off and the wave is allowed to evolve freely for seven more days. A range of forcing phase speeds and amplitudes are used, but two simulations are presented in detail. One has a flow-relative forcing phase speed of 55 m s^{-1} and the other of zero, and both have maximum forcing amplitude of 10 K d^{-1}. Both of these forcings produce waves which are initially rapidly damped, but then settle in to quasi-steadily propagating, coherent configurations which are weakly decaying or neutral. The authors focus on this latter period. The faster forcing produces a convectively coupled gravity wave qualitatively similar to those predicted by strict quasi-equilibrium (SQE) theory, but whose interaction with convection is weaker than that theory predicts. The adiabatic cooling is considerably larger than the diabatic heating, and consequently the phase speed is roughly 30 m s^{-1} rather than the $10-15$ m s^{-1} typically predicted by SQE for waves of this vertical structure. Sensitivity studies show that this wave, when propagating eastward against a mean westward flow, is destabilized by linear evaporation-wind feedback. The slower forcing produces a wave which is stationary in the mean flow frame and does not have the structure of a gravity wave. This wave has a much larger signal in the moisture field than does the faster wave, and much closer cancellation between adiabatic cooling and diabatic heating. This wave appears similar to ones appearing in some recent theoretical studies and cloud-resolving simulations.

1. Introduction

This study addresses the interaction of deep moist convection with relatively large-scale waves in a nonrotating atmosphere. To do this, we impose waves on a mesoscale model simulation with idealized boundary conditions which has been previously brought to a state of approximate radiative–convective equilibrium. The aim is to evaluate the relevance of various mechanisms of interaction between waves and convection which have been proposed. Specifically, we examine the phase speed reduction and moist convective damping which strict quasi-equilibrium (SQE) theory, as presented by Emanuel, Neelin, and Bretherton (1994, hereafter ENB), predicts. We also find a mode of behavior that appears to be fundamentally associated with the moisture field, and that bears some

*Corresponding author.
e-mail: ahs129@columbia.edu

resemblance to modes discussed in recent theoretical studies (Sobel et al., 2001; Fuchs and Raymond 2002).

Ideally, we would like to use a cloud-resolving model for this purpose, as a mesoscale model (essentially by definition) has a convective parameterization and hence makes some assumptions about the nature of the interaction between convection and larger-scale motions. However, a mesoscale model is computationally lighter. The convective parameterization used here, that of Kain and Fritsch, is relatively sophisticated and complex by comparison to those used in theoretical studies. To some degree it can be considered theoretically agnostic, in the sense that it was not designed to give any particular result in the idealized context in which we use it here, and it is not straightforward to predict what it will do in this situation.

This study follows a prior one by Su, Bretherton, and Chen (2000, hereafter SBC) who used the Penn State/National Center for Atmospheric Research Mesoscale Model (MM5) to examine whether deep convection over a horizontally uniform tropical ocean, with doubly periodic boundary conditions and an imposed mean lifting, would "self-aggregate" on large scales in the absence of horizontally inhomogeneous forcings. They found that self-aggregation did occur when the mean lifting had a "top-heavy" profile, but did not otherwise. In the present study, we use a model very similar to that of SBC, but rather than looking for self-aggregation, we impose large-scale wavelike disturbances on a mean state of approximate radiative–convective equilibrium with no domain-averaged vertical motion. Our simulations also differ from those of Su et al. in that we use fixed radiative cooling rather than an interactive radiation scheme. This is done in order to focus on the interaction of large-scale gravity wave dynamics and deep convection in the model, without the complicating (but potentially important, in reality) effects of radiative–convective feedbacks. Given the multiplicity of physical mechanisms interacting in the real system, we take the view that it is sensible to try to understand feedbacks between limited subsets of those mechanisms before attempting to understand the entire system. However, the removal of radiative–convective feedbacks (in addition to the caveats that must always be applied when using a model with particular physical parameterizations to understand the interaction of large-scale dynamics with convection) strongly limits the direct applicability of our results to the real atmosphere.

2. Model and experimental configuration

We present only a brief description of the model here; further details can be found in SBC and in Grell et al. (1994). The fluid dynamics are nonhydrostatic and compressible, and are solved with a finite difference method. The sound wave terms are integrated separately from the rest of the terms in the equation of motion using a semi-implicit scheme. The Kain–Fritsch convective parameterization (Kain and Fritsch, 1990, 1993; see also Fritsch and Chappell, 1980; Fritsch and Kain 1993) is used. This is a "hybrid" scheme (Frank and Cohen, 1987; Cohen and Frank, 1987; Molinari and Dudek, 1992; Frank, 1993; Molinari, 1993; Kain and Fritsch, 1998) in that it exchanges condensate with the explicit moisture scheme as well as supplying heating and drying tendencies to the larger model. The explicit moisture scheme (Dudhia, 1989) carries only two condensate variables, which represent cloud water and rain water for temperatures greater than 0 °C, and cloud ice and snow for temperatures less than 0 °C. The fall speed of cloud ice in the explicit moisture scheme has, as in SBC, been modified according to Heymsfield and Donner (1990). The boundary layer scheme is Zhang and Anthes' (1982) version of the scheme of Blackadar (1976, 1978).

The vertical coordinate is $\sigma = (p - p_t)/(p_s - p_t)$, with p the pressure, p_s the surface pressure, and $p_t = 50$ hPa. We run the model with 24 vertical levels, corresponding to a vertical resolution of $\sigma = 0.05$ throughout most of the troposphere, but higher resolution in the boundary layer. Horizontal grid spacing was set to 30 km. The horizontal domain size is 40×150 grid points, or 1200×4500 km, with doubly periodic boundary conditions as in SBC. Radiative cooling is fixed at 2 K d^{-1} below $\sigma = 0.3$, and then decreases linearly in σ to zero at $\sigma = 0.1$ and above. As in SBC, the model's horizontally averaged momentum field is continually relaxed with a 2 h time scale towards a profile with 5 m s^{-1} easterly winds throughout the troposphere. This forcing does not affect wind variations having any horizontal structure. The lower boundary condition for the model is an ocean surface with a fixed temperature of 29 °C. A radiative upper boundary condition is used (Klemp and Durran, 1983).

The initial state for all the wave simulations in this study was produced as follows. The model was initialized with all fields horizontally uniform, with temperature and moisture following a TOGA COARE mean sounding, except for random noise added to the lowest

model level's temperature field. This simulation is then run with no forcing on the thermal fields other than the fixed radiative cooling for 16 days, by which time the model has reached a state of approximate radiative–convective equilibrium. Convection is quite evenly distributed throughout the domain in this state, with no large-scale structure (i.e., no self-aggregation occurs, consistent with SBC's result that a top-heavy mean lifting is required).

From this initial state, we performed a set of simulations in which, starting on day 17, we imposed a wave-like heating on the temperature field, of the form

$$Q = Q_0 F(\sigma) \sin[2\pi(x - ct)/L] \tag{1}$$

where L is the domain length, 4500 km, and

$$F(\sigma) = \sin\left(\frac{\pi(1-\sigma)}{1-0.15}\right), \quad \sigma > 0.15$$
$$F(\sigma) = 0, \quad \sigma < 0.15. \tag{2}$$

Our various experiments differed only in the choices of the heating amplitude Q_0 and phase speed c. The vertical structure of the forcing was designed to stimulate the gravest vertical mode of the troposphere, assuming such a thing can be defined for this moist system. In fact, defining the linear (let alone nonlinear) modes of this system, with all the physics included, from the known model equations is a difficult task, and we do not attempt it. The form of eqs. (1) and (2) was simply an educated guess, but we will see below that in some cases this forcing was able to excite fairly clean modal structures in the model. We chose Q_0 to be either 10 or 2 K d^{-1}. We tried three values for c: 50, 10, and -5 m s^{-1}, where the minus denotes an easterly direction. These values, to which 5 m s^{-1} should be added to obtain the intrinsic, or flow-relative phase speed, correspond respectively to approximate guesses for a dry first baroclinic mode phase speed, a reduced phase speed as predicted by quasi-equilibrium theory, and an advective intrinsic phase speed of zero. We will only discuss in detail the simulations with forcing phase speeds of 50 and -5 m s^{-1}, as the 10 m s^{-1} phase speed did not excite a very coherent wave. The reason for this may perhaps be gleaned from the faster phase speed simulation, which seems to show that the natural moist gravity wave phase speed for wavelength L in this model is nearer 30 m s^{-1}.

3. Results

For two of the simulations, we present several figures based on Fourier spectral decomposition of the model fields to extract the component with wavenumber 1 in x and wavenumber zero in y, i.e., that which matches the forcing.

3.1. Fast forcing: convectively coupled gravity wave

For the simulation with $Q_0 = 10$ K d^{-1} and $c = 50$ m s^{-1}, Fig. 1 shows the amplitude and phase of this component, as a function of time, in four two-dimensional fields: the surface hourly rainfall and the temperature at three different levels, $\sigma = 0.995$ (the lowest model level), 0.705, and 0.305. On the x–axis of this figure as well as Figs. 3 and 7, hour "0" refers to the time at which the forcing is turned on. The amplitudes are normalized so that the largest value shown for each field is unity. A sense of the actual amplitudes can be obtained from the composites in the next figure. We see that in this simulation, we have managed to excite an essentially pure single mode of the system; the structure propagates with constant phase relations between the different fields for the whole 7 days after the forcing is turned off. This is the cleanest example of this which we obtained in all our simulations (only a subset of which are shown in this paper). For an arbitrary choice of Q_0 and c, the phase relations between the fields shown here generally change considerably more than this throughout the simulation. The progression of the phase yields an estimate of the phase speed of approximately 30 m s^{-1}, slower than one expects for a dry gravity wave with this vertical structure but considerably faster than most estimates of reduced moist gravity wave phase speeds, both from theory (e.g. ENB) and observations (Wheeler and Kiladis, 1999).

The amplitude shows vacillation superimposed on overall rapid decay after the forcing is turned off. Given that most of the convective heating in these simulations is parameterized rather than explicit, and that the Kain–Fritsch scheme is constructed explicitly to reduce CAPE fairly rapidly, it seems justified to ascribe this decay to the phenomenon of "moist convective damping" as described by ENB. During the last few days of the simulation, on the other hand, when the amplitude is relatively small, it appears to be nearly statistically steady in time, rather than continuing to decay with an e-folding time comparable to that of the earlier part of the simulation.

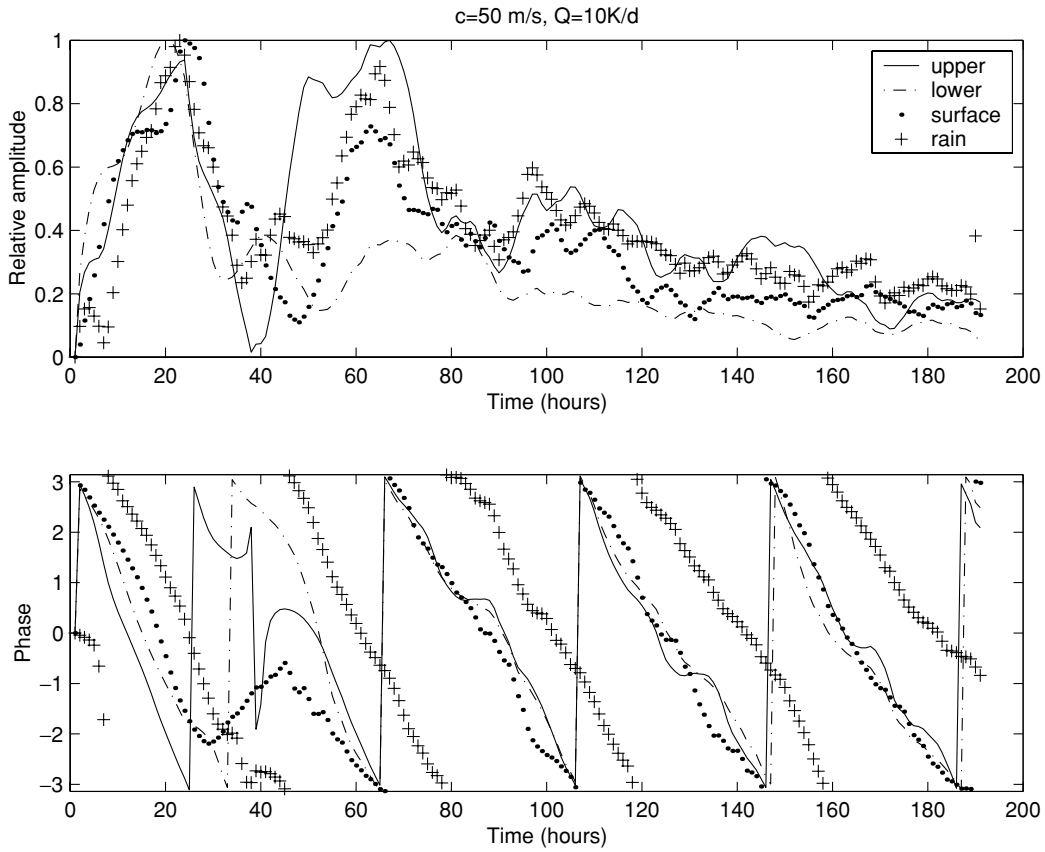

Fig. 1. Time series of the amplitude and phase of the x ("zonal") wavenumber 1, y (meridional) wavenumber 0 component of the temperature field at $\sigma = 0.995$ ("surface"), 0.705 ("lower"), 0.305 ("upper"), and the surface precipitation field, for the simulation with an initial forcing phase speed of 50 m s $^{-1}$ and amplitude of 10 K d^{-1} (convectively coupled gravity mode).

Figure 2 shows composites of the wave structure, constructed using the phase of the wave's temperature anomaly at $\sigma = 0.705$ to define the wave phase for all the fields at any given time. As might be guessed from the time series, using a different level as the basis for the composites does not significantly alter the composite wave's structure. We show the temperature, horizontal (zonal) and vertical velocities, and convective heating. The flow and temperature structures are clearly gravity wave-like, with propagation to the "east" (right) as dictated by the initial forcing. We refer to this wave hereafter as a convectively coupled gravity wave, or as the "fast mode". The convective heating is roughly collocated with the vertical motion, as we might expect, but with a slight lag of 5–10% of a wavelength. Qualitatively, this structure is as SQE theory, according to ENB, predicts. However, in this theory and in observations of tropical waves, the convective heating perturbations nearly counterbalance the adiabatic cooling associated with vertical motions. This greatly reduces the response of the temperature field to the vertical motions, producing a small effective static stability and a slow baroclinic convectively coupled gravity wave speed.

Figure 3 shows the linear vertical advection of potential temperature, $w'\partial\bar{\theta}/\partial z$, for comparison to the diabatic heating for this mode (lower right panel of Fig. 2). The adiabatic cooling is larger by a factor on the order of four or so (though this varies with height) than the convective heating. Hence, while the qualitative interaction between the wave and the convection is as predicted by ENB, when the wave amplitude is small the interaction is quantitatively weaker than those authors' arguments suggested. This is consistent

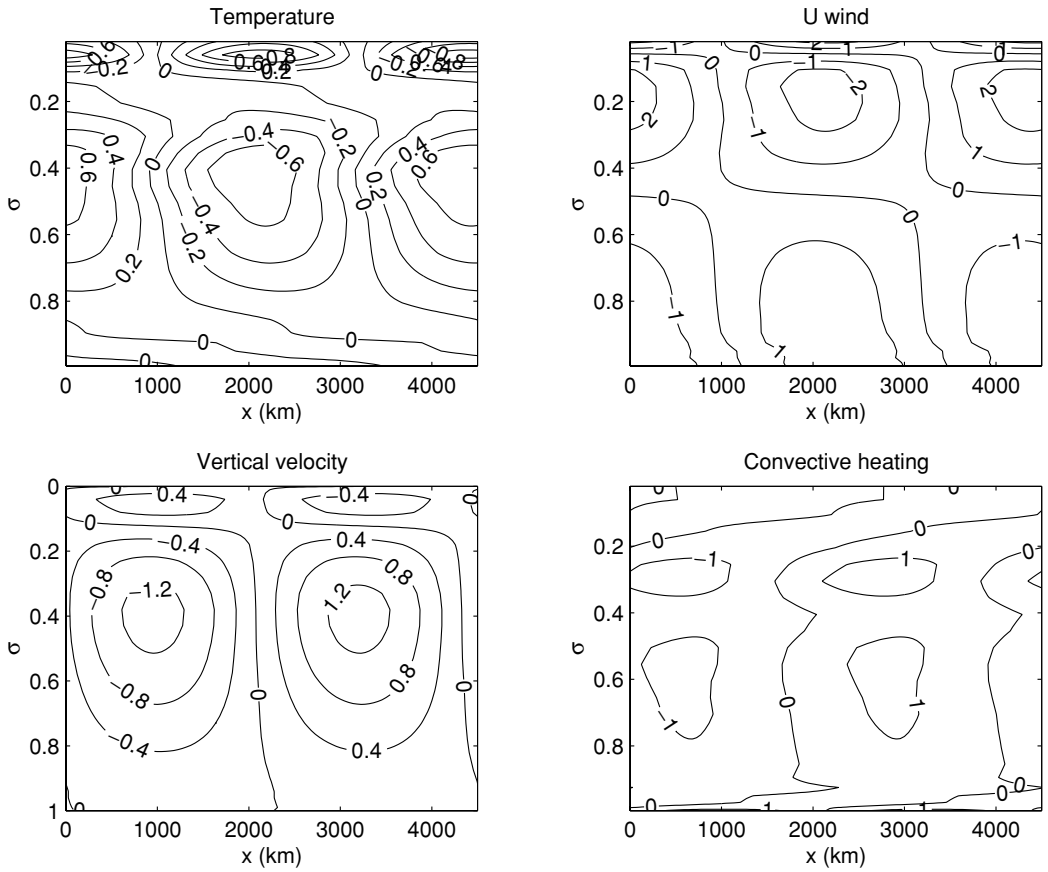

Fig. 2. Wave composite (see text for details of the calculation by which this was obtained) for the simulation with an initial forcing phase speed of 50 m s^{-1} and amplitude of 10 K d^{-1} (convectively coupled gravity mode). Panels show the temperature (K), x ("zonal") velocity (m s^{-1}), vertical velocity (cm s^{-1}), and convective heating (K d^{-1}).

with the phase speed's being greater and moist convective damping weaker than in ENB's results, as shown in Fig. 1. The moist convective damping is much larger earlier in the simulation when the amplitude is large, but as ENB (like most theoretical studies of convectively coupled waves) used linear theory, a comparison at small amplitude is appropriate. Further discussion of the phase speed is given in section 5.

3.2. Slow forcing: stationary moisture wave

Figures 4 and 5 show results analogous to those Figs. 1 and 2, but for the simulation with initial forcing phase speed equal to the mean flow speed, -5 m s^{-1}. There are some similarities, but also some striking differences with the simulation shown above. The time series, though quite different in detail, show large amplitudes (with strong oscillations) in the first half of the simulation, settling down to a lower-amplitude, quasi-steadily propagating pattern in the latter half. The phase relationships are different than in the previous case: in the first half of the simulation, there is much less apparent coherence between the different time series, while in the latter half of the simulation, the lower and surface temperatures are in phase with each other but roughly 180° out of phase with the upper tropospheric ($\sigma = 0.305$) temperature and rainfall. These phase relationships are commonly found in observations of a variety of tropical disturbances. The phase speed in the latter half of the simulation is essentially the same as that of the initial forcing (and the mean flow).

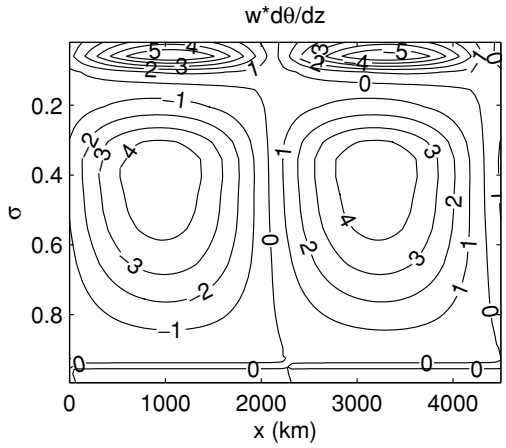

Fig. 3. Wave composite of the linear vertical advection of potential temperature (K d^{-1}) for the simulation with an initial forcing phase speed of 50 m s^{-1} and amplitude of 10 K d^{-1} (convectively coupled gravity mode). Compare to the convective heating for the same mode, shown in the lower right panel of Fig. 2.

The composite (Fig. 5) also shows significant differences with the previous simulation. Most significantly, the vertical velocity is now concentrated in the upper troposphere, and is almost exactly out of phase with the temperature, rather than being in quadrature. This structure does not resemble a propagating gravity wave. There is also a much higher degree of cancellation between adiabatic cooling, shown in Fig. 6, and diabatic heating, shown in the lower right panel of Fig. 5. Because this wave is stationary with respect to the mean flow, and has a large signal in moisture fields (see below) we refer to it as a "stationary moisture wave", or the "slow mode".

3.3. Moisture fields

Figures 7 and 8 show wave composites for the two simulations of several moisture-related fields: relative humidity, precipitation, precipitable (i.e., column-integrated) water vapor, and virtual temperature. In both cases, the precipitation and precipitable water vapor are in phase with each other and with the vertical velocity, and the temperature and relative humidity are out of phase. However, in the "slow mode" the relative humidity signal is considerably larger in amplitude and deeper in vertical structure, and correspondingly the precipitable water vapor signal is an order of magnitude larger than in the "fast mode". The precipitation rate perturbations are of the same order of magnitude in the two simulations, but somewhat larger at about 4 mm d^{-1} in the slow simulation compared to about 2.6 in the fast one.

Comparing the virtual temperature composites in Figs. 7 and 8 to the temperature composites in Figs. 2 and 5, we see that the virtual temperature correction is negligible for the fast mode but quite significant for the slow mode, in the latter case reducing the amplitude and at some levels reversing the sign of the anomaly. This is energetically important because the vertical eddy temperature flux, $\overline{w'T'}$, for the slow mode is strongly negative, which would lead one to expect a strongly damped temperature signal, contrary to what we see in the simulation. The virtual temperature flux $\overline{w'T'_v}$, on the other hand, is smaller than $\overline{w'T'}$ by a factor of 6, and smaller for the slow mode than the fast mode. For both modes, the troposphere and phase-averaged kinetic energy $\langle\overline{e}\rangle$ is roughly 1 m^2 s^{-2}. The buoyancy flux $\overline{w'b'} = g\overline{w'T'_v}/\overline{T}$, which is the principal source/sink of wave kinetic energy, has a tropospheric average of about -2×10^{-6} m^2 s^{-3} for the fast mode, and half that for the slow mode. This yields rather slow decay timescales of $\langle\overline{e}\rangle/\langle\overline{w'b'}\rangle \approx 5-10$ d, so both waves can be considered quasi-neutral on timescales of a few days.

4. Role of surface flux feedbacks

In models of tropical moist large-scale dynamics which are based on quasi-equilibrium principles (here generally defined as the notion that convection is solely a response to instability in the local thermodynamic sounding, and acts to remove such instability, e.g., Arakawa and Schubert (1974; ENB; Neelin and Yu 1994; Fuchs and Raymond, 2002), the interaction between convection and large-scale fluid dynamics generally does not by itself produce unstable modes. Additional physical processes are generally needed to do this, and the primary candidates which have been identified are feedbacks with surface fluxes (Emanuel, 1987; Neelin et al., 1987; ENB) and cloud–radiative interactions (e.g., Raymond, 2000; Fuchs and Raymond, 2002). The latter is explicitly turned off in our simulations, but the former is not. We performed sensitivity experiments to determine whether surface flux feedbacks are playing a role in the simulations described above.

We performed tests in which surface flux feedbacks are completely eliminated by a procedure used in SBC.

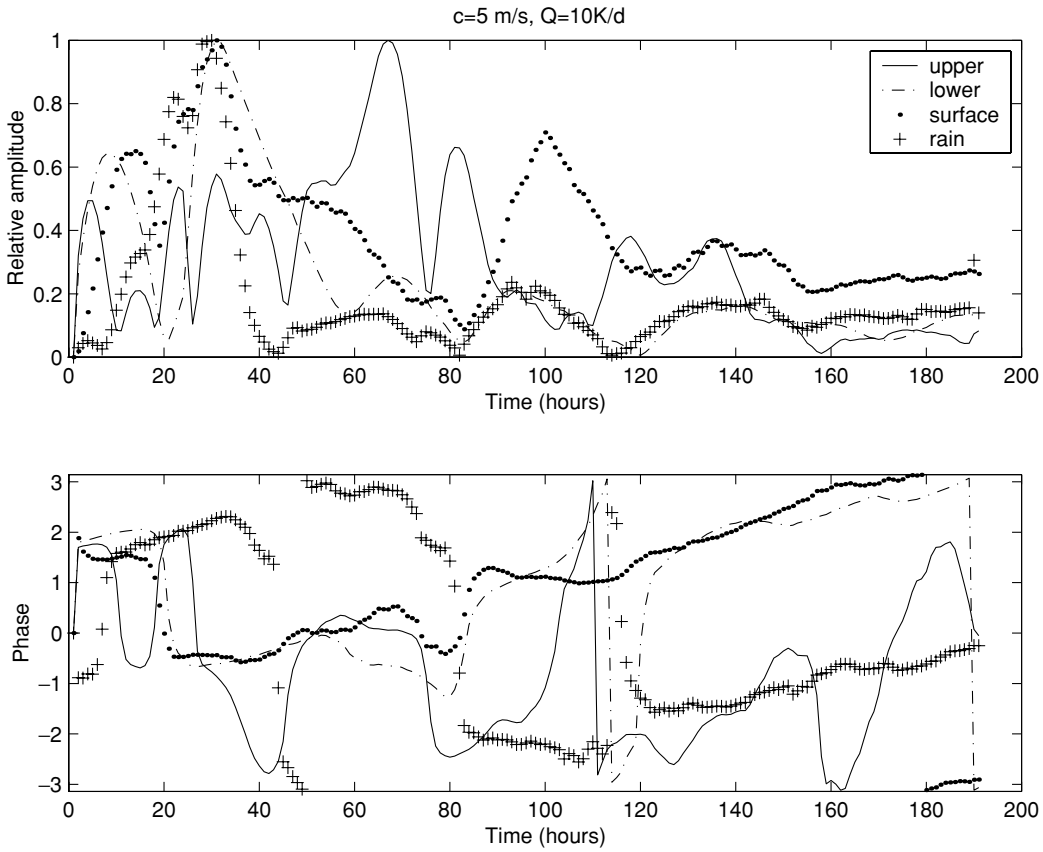

Fig. 4. Time series, as in Fig. 1, but for the simulation with an initial forcing phase speed of -5 m s^{-1} and amplitude of 10 K d^{-1} (stationary mode).

At each time step, the surface fluxes are computed normally, but before applying those fluxes to the model equations, the fluxes are averaged horizontally over the whole domain. Thus, the domain-averaged fluxes are unchanged, but the fluxes are rendered horizontally uniform and thus unable to interact with the wave.

In the case of the stationary moisture mode (forcing phase speed of -5 m s^{-1}), the effect of this surface flux averaging was to slightly increase the wave's amplitude with very little change in its structure. We do not show the results for this case, as the preceding sentence is essentially adequate to describe them. Clearly this wave is not enhanced by surface flux feedbacks.

The fast gravity wave (forcing phase speed of 50 m s^{-1}) responded quite differently to this test. Figure 9 shows the time series plot for this simulation, to be compared to Fig. 1. The persistent, very coherent wave structure evident in Fig. 1 falls apart after a few days when the surface flux feedback to the wave is turned off. Towards the end of the simulation, in fact, a westward-propagating signal reminiscent of the stationary moisture wave emerges, but it is not coherent in the temperature at all levels. We have created a composite wave plot analogous to Fig. 2 for this simulation, but because of the lack of coherence in both space and time during the last few days of the simulation it is not particularly meaningful and hence not shown. However, the anomalies in all fields are smaller than those in Fig. 2, typically by a factor of two or more. We conclude that the convectively coupled gravity wave in the original simulation (shown in Figs. 1 and 2) *is* enhanced by surface flux feedbacks.

Most explicit discussion of these feedbacks has focused on the role of surface wind perturbations, as

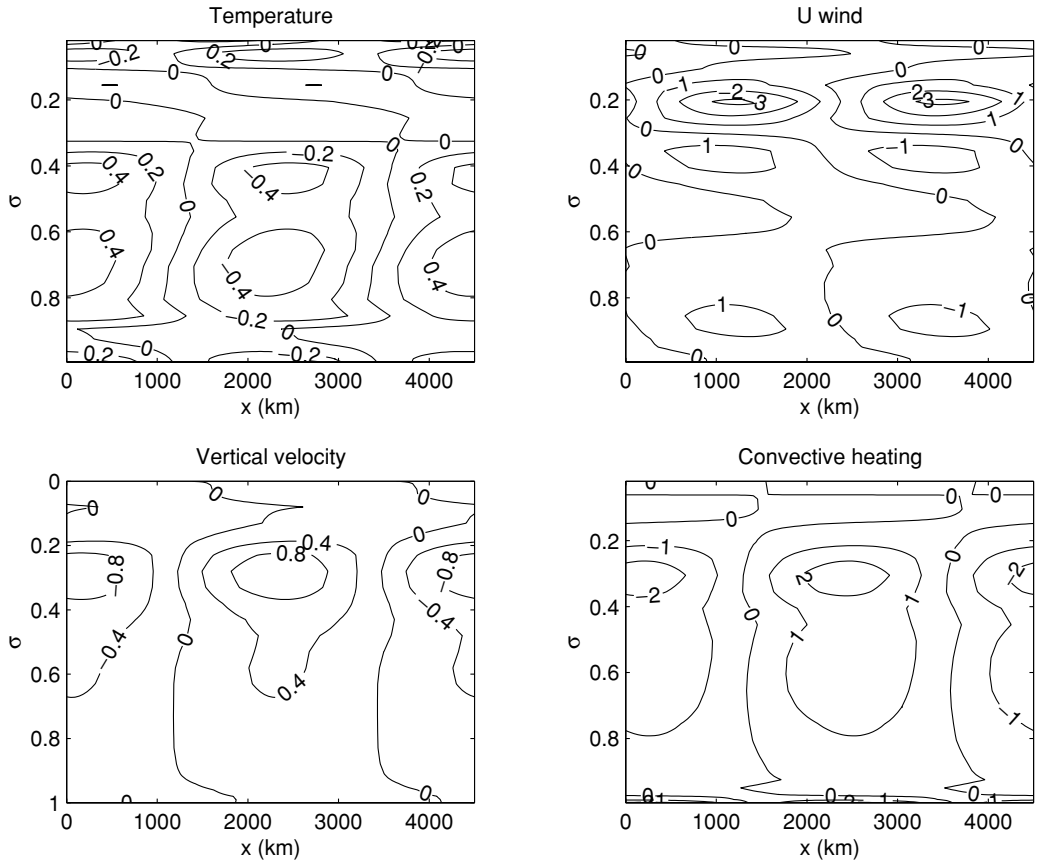

Fig. 5. Wave composite as in Fig. 2 but for the simulation with an initial forcing phase speed of -5 m s^{-1} and amplitude of 10 K d^{-1} (stationary mode).

opposed to perturbations in surface atmospheric temperature and humidity, in generating surface flux anomalies. Figure 2 shows that for this wave, surface wind anomalies are $\sim$1 m s^{-1}, or about 20% of the mean wind speed, while surface anomalies in temperature and humidity are very small. This suggests that the enhancement of the wave is due to evaporation–wind feedback (Neelin et al., 1987), also known as wind-induced surface heat exchange (WISHE; Emanuel, 1987, 1993).

Examination of the wind anomalies in Fig. 2 shows anomalous easterlies (which add to the mean wind to produce a net enhancement of the surface wind speed) ahead of the heating maximum. Concurrent examination of the heating and moisture fields suggests that the surface flux enhancement helps to produce the low-level positive moisture anomaly ahead of the heating maximum. The heating maximum is nearly a quarter-wavelength ahead of the temperature minimum, but is shifted slightly back towards the minimum, consistent with weak damping. We hypothesize that the low-level moisture maximum is created by the surface wind speed maximum, and that this shifts the convection "forward" away from the cold phase of the wave, thus reducing the moist convective damping. The experiment with surface fluxes averaged might be thought of as a test of this, and indeed in that experiment the heating was nearly directly in the cold phase of the wave, but because of the greatly reduced coherence of the wave signal this is not a very good test.

To test this further, we performed an experiment in which the initial forcing phase speed was -60 m s^{-1}, i.e., the same in flow-relative magnitude as in

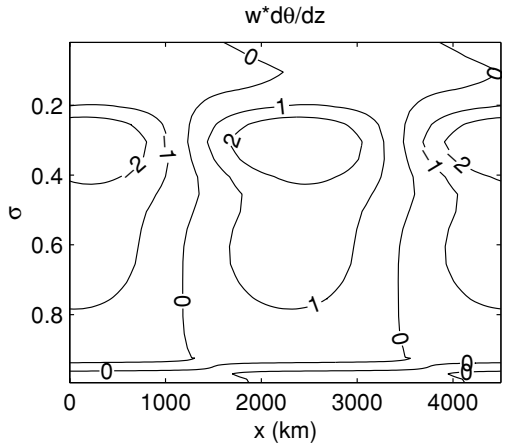

Fig. 6. Wave composite of the linear vertical advection of potential temperature (K d^{-1}) for the simulation with an initial forcing phase speed of -5 m s^{-1} and amplitude of 10 K d^{-1} (stationary mode). Compare to the convective heating for the same mode, shown in the lower right panel of Fig. 5.

the 50 m s^{-1} case, but opposite in direction. In this simulation, the surface fluxes are computed in the normal way, with no horizontal averaging applied. The evaporation–wind feedback mechanism, if important here and if acting in a fundamentally linear way (so that it depends on the addition of wave-induced surface wind anomalies to the mean surface wind), should be damping rather than destabilizing. The time series for this case (not shown) shows wave amplitude decaying considerably more rapidly than in the eastward-propagating case, indicating that in that case the surface flux enhancement of the wave does indeed occur due to an essentially linear evaporation–wind feedback.

5. Interpretation in terms of other simple linear models

5.1. Context

We have identified two distinct modes in our simulations, a convectively coupled gravity wave and a stationary mode with a large signal in the humidity field. The analytical model of ENB contains an analog of only the former, but more recent theoretical studies have identified modes which are analogous to the latter. These studies enable us to place our simulations in context, and in turn the simulations provide estimates of the parameters which appear in the theoretical studies.

Sobel et al. (2001) analyzed the equations of the "Quasi-equilibrium tropical circulation model" (QTCM; Neelin and Zeng, 2000; Zeng et al., 2000) under the "weak temperature gradient (WTG) approximation" in which diabatic heating and adiabatic cooling balance exactly and temperature perturbations are neglected at leading order. Gravity waves are filtered out by this approximation. Those authors also linearized the equations and ignored the effects of perturbations in surface fluxes and radiative heating. The resulting waves depended only on the modulation of convection by the moisture field, which then feeds back on the moisture field as the convective heating perturbations drive flow perturbations which in turn advect the moisture field. In the nonrotating case, the only mode has zero flow-relative phase speed and is damped on a time scale $\tau_c M_q / M$, where τ_c is a convective adjustment time scale as in the Betts–Miller parameterization (Betts, 1986; Betts and Miller, 1986), M_q is the gross moisture stratification and M the gross moist stability (Neelin and Held, 1987; ENB; Neelin, 1997; Neelin and Zeng, 2000; see also the appendix below).

Fuchs and Raymond (2002) analyzed a linear model which, although constructed on assumptions which are in principle somewhat different, bears much formal similarity to the linearized QTCM equations. Fuchs and Raymond paid much attention to the effects of radiative–convective feedbacks and surface flux feedbacks, but also considered the case in which both these feedbacks are inactive. This limit is most relevant to our stationary moisture wave, and also to the analysis of Sobel et al. (2001). Fuchs and Raymond's model has two convective time scales, one for temperature and one for moisture, rather than one as for the QTCM. In their model the precipitation, P, is modeled by [cf. their eq. (18)]

$$P = \frac{2}{m}(\alpha Q - \mu B) \tag{3}$$

where m is the vertical wavenumber, Q the amplitude of the moisture perturbation, B the mid-tropospheric temperature perturbation, and α and μ rate constants with units of inverse time. In the linearized QTCM, the precipitation is

$$P = \frac{(q - T)}{\tau_c} \tag{4}$$

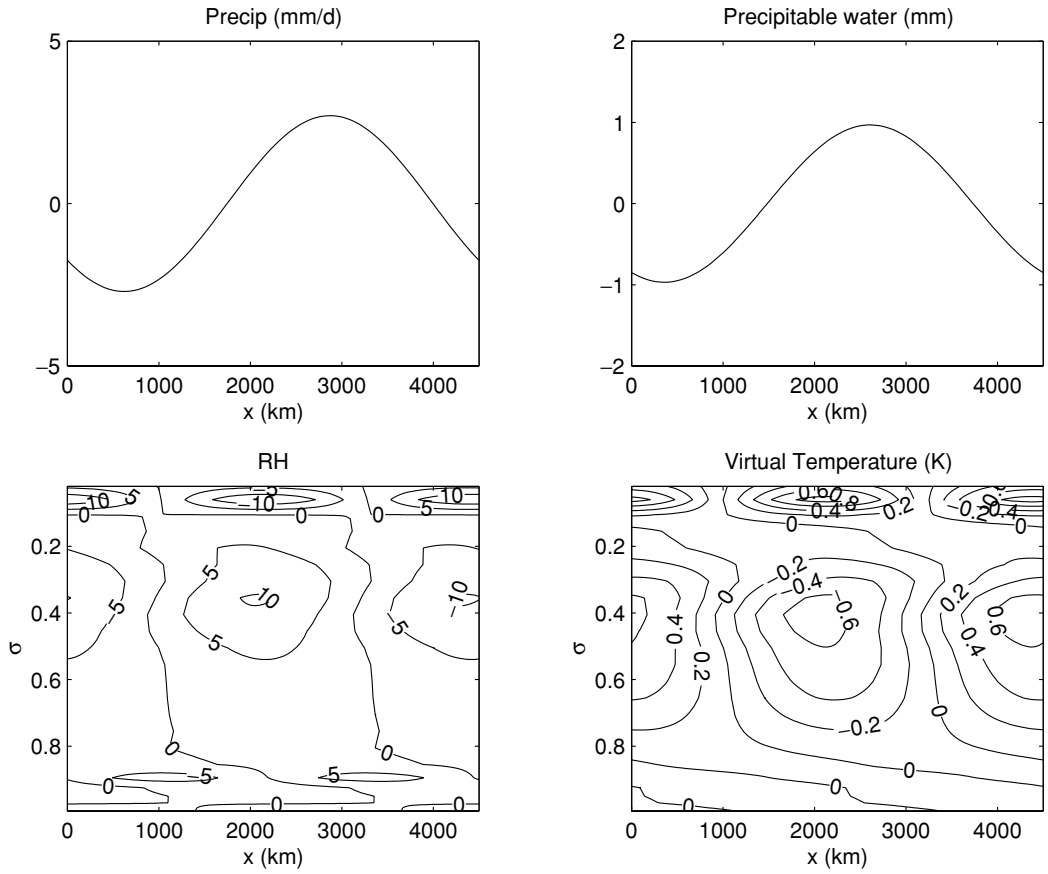

Fig. 7. Wave composite as in Fig. 2, for the simulation with an initial forcing phase speed of 50 m s^{-1} and amplitude of 10 K d^{-1}W (convectively coupled gravity mode), but showing precipitation (mm d^{-1}) precipitable water vapor (mm), relative humidity (percent), and virtual temperature (K).

where q and T are the moisture and temperature perturbations. The vertical basis functions used for q and T are different from those used for Q and B, but at a fixed m, clearly eqs. (3) and (4) can be made equivalent by the choices $\alpha = \mu = \tau_c^{-1}$ and the correspondence $(2/m)(Q, B) \rightarrow (q, T)$.

Fuchs and Raymond identify two basic modes in their analysis: a stationary mode and a convectively coupled gravity wave mode. These appear to correspond to our two modes. The convectively coupled gravity mode is similar in some aspects of its dynamics to those identified previously in quasi-equilibrium theories (e.g., ENB). The stationary mode (with radiative–convective and surface flux feedbacks turned off) resembles the nonrotating modes studied by Sobel et al. (2001) as well as the long-lived stationary anomalies in moisture and convection simulated by Tompkins (2001) with a cloud-resolving model, and our stationary moisture wave. We consider this wave first.

5.2. *Stationary moisture wave*

As mentioned above, Sobel et al. (2001) find in the QTCM equations under WTG that the stationary mode is damped on a time scale $M_q \tau / M$. In Fuchs and Raymond's model, the stationary mode is always stable if radiative–convective and surface flux feedbacks are inactive, and at high horizontal wavenumber, their analysis produces a damping rate identical to that obtained by Sobel et al. (2001). However, the mode of Fuchs and Raymond becomes much more strongly damped at low wavenumber, presumably due to the breakdown of the WTG approximation at spatial scales larger than the deformation radius (see Sobel et al.,

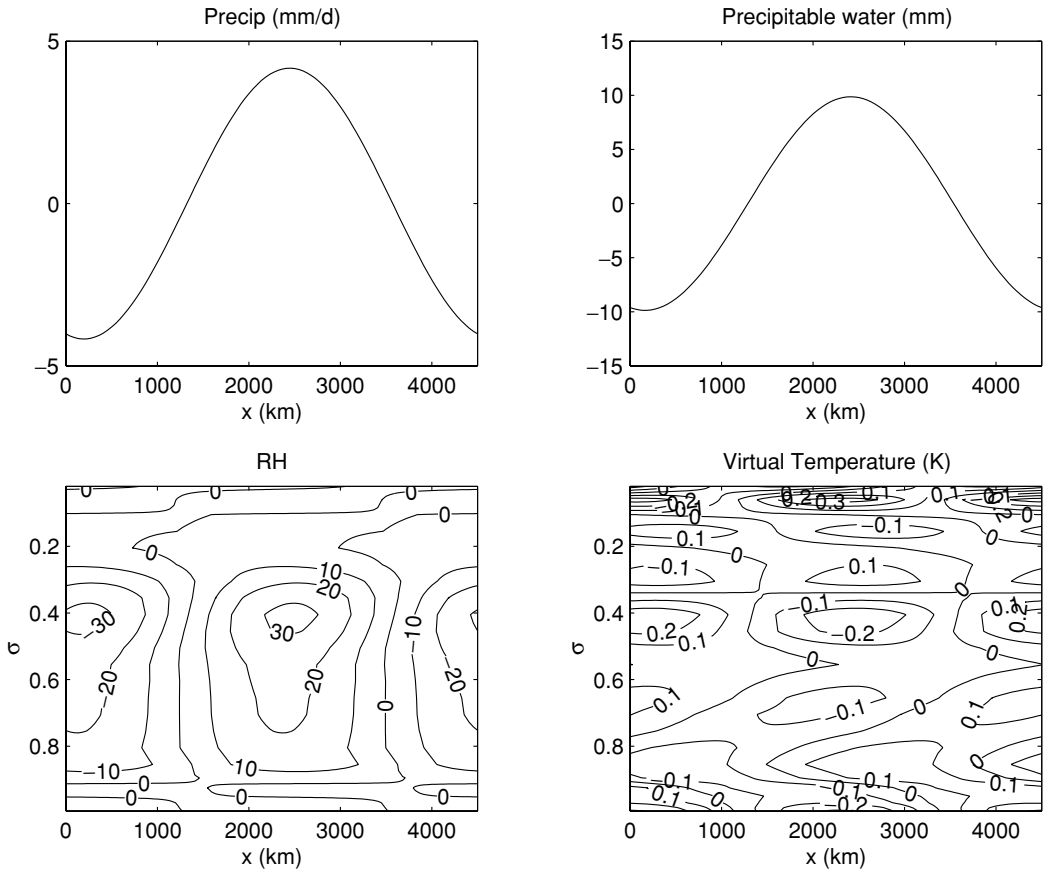

Fig. 8. As in Fig. 7, but for the simulation with an initial forcing phase speed of -5 m s^{-1} (stationary mode).

2001). The transition occurs at a wavenumber whose value depends sensitively on α and μ, neither of which is very precisely known. Our stationary mode (advective moisture wave) in the MM5 is clearly damped only weakly, or may even be neutrally stable. Therefore in this model, it appears that if this transition exists, it occurs at a scale larger than 4500 km. At least for wavelengths smaller than this (and possibly larger) the high-wavenumber regime of Fuchs and Raymond, which corresponds to the results of Sobel et al. (2001), appears most relevant.

We can use this mode to estimate an effective value of Fuchs and Raymond's moisture time scale α^{-1}, which plays a role equivalent to τ_c in the QTCM under the weak temperature gradient approximation. Fuchs and Raymond neglected virtual effects on density, but their temperature perturbation B should be interpreted as a buoyancy, or virtual temperature perturbation. The virtual temperature anomaly was shown in Fig. 8 to be very small. Therefore, we can neglect B in eq. (3) or T in eq. (4), and fit these formulae to our simulation by simply dividing the precipitable water anomaly by the precipitation anomaly to obtain an α^{-1} of approximately 2.5 d. This is 2.5 times larger than that assumed by Fuchs and Raymond (though they carefully considered the sensitivity to this parameter), and 30-fold larger than the 2 h used in the simplified Betts–Miller scheme of the QTCM.

To check whether this time scale is consistent with the observed quasi-neutral wave evolution, we evaluate the factor M_q/M directly from the wave composite fields. Typically M is computed in terms of a known vertical basis function for the vertical velocity (e.g., Neelin, 1997; Yu et al., 1998). We wish to use the observed large-scale vertical velocity from the wave rather than a prescribed basis function. A way of doing

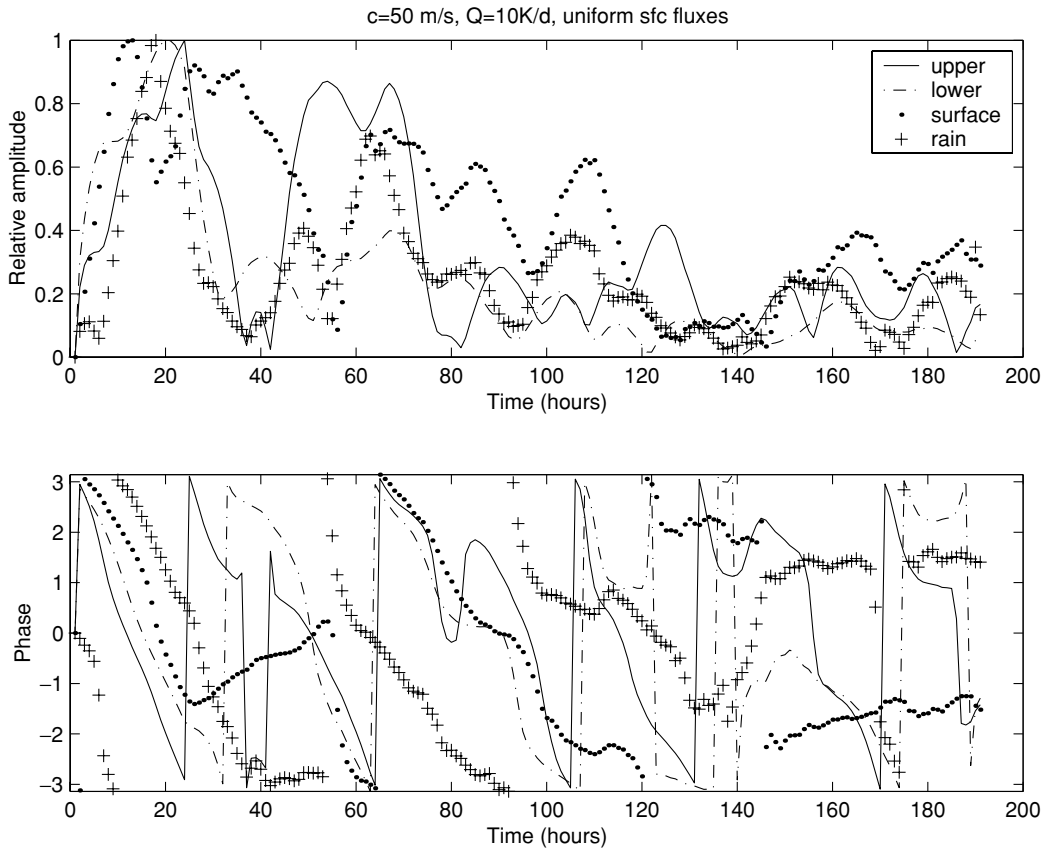

Fig. 9. Time series, as in Fig. 1 (convectively coupled gravity mode), but for the simulation with horizontally averaged surface fluxes (see text for details).

this which allows direct comparison between results using an arbitrary vertical velocity profile is in terms of the ratio of M and its dry counterpart, M_S, since both incorporate the same vertical velocity profile in this calculation so that its magnitude cancels. We compute M/M_S as follows:

$$\frac{M}{M_S} = \frac{\int_{p_t}^{p_s} \omega \frac{\partial h}{\partial p}\, \mathrm{d}p}{\int_{p_t}^{p_s} \omega \frac{\partial s}{\partial p}\, \mathrm{d}p} \tag{5}$$

where p_s and p_t are the pressures at the surface and top of the convective circulation respectively, ω is the pressure vertical velocity, s and h the dry and moist static energies respectively. M_q is also determined by this computation since $M_q = M_S - M$.

Using eq. (5) to compute the ratio M/M_S on a section through the maximum positive precipitation anomaly of the composite for this wave yields a value of approximately 0.23 (variations of around $0.01-0.02$ can be induced by varying the assumed value of p_t by a model level or two; our baseline choice is $\sigma = 0.155$), implying that the ratio M_q/M is around 4, and thus that the decay time scale for the wave should be around 10 d, based on the estimate for α^{-1} of 2.5 d obtained above. This is consistent with the nearly neutral evolution that we observe over the last 4 days of the simulation, and also agrees quite well with the decay time scale deduced from energetic considerations in section 3.3.

5.3. Convectively coupled gravity wave

As shown above, the mode we generate by an initial forcing phase speed of 50 m s^{-1} has the characteristics of a convectively coupled gravity wave which is destabilized (though not to the point of being actually

unstable) by the evaporation–wind feedback. Qualitatively, the phase relationships between heating, temperature, and vertical motion anomalies are just as one would expect from SQE theory such as presented in ENB. However, the strength of the interaction between convection and gravity wave dynamics is considerably weaker than that theory predicts. The wave-induced diabatic heating is considerably less than the adiabatic cooling, and so the phase speed reduction is considerably less drastic than in ENB and similar studies. However, Fuchs and Raymond do obtain phase speeds as large as 30 m s^{-1} (at long wavelengths) for convectively coupled gravity waves destabilized by evaporation–wind feedback.

For this wave, computing M/M_S on a section through the maximum positive precipitation anomaly gives a value of about 0.35. Using SQE theory as in ENB with an assumption of fixed relative humidity yields a phase speed smaller than the dry one by a factor of $\sim 0.5(M/M_S)^{1/2}$, as shown in the appendix, or about 15 m s^{-1} assuming a dry gravity wave phase speed of 50 m s^{-1}. However, Figs. 2 and 7 show that constant relative humidity, and the uniform convective available potential energy (CAPE) across wave phase (note the lack of temperature and moisture variation in the PBL, while the free tropospheric virtual temperature varies by $\sim$0.5 K) assumed under SQE, are poor assumptions. A more appropriate approximation for this mode is to assume that variations in column-integrated moisture are negligibly small, and a simple modification of the SQE argument to this effect yields a phase speed equal to $(M/M_S)^{1/2}$ times the dry phase speed, or 30 m s^{-1}, in good agreement with the "observed" phase speed in the simulation.

Again, we can attempt to use the simulation to estimate the convective time scale(s) from the simple theoretical models described above, but the attempt is somewhat less successful than in the previous case. We can estimate Q and B by integrating the temperature and moisture anomalies shown in Fig. 2 in height. Doing this at a horizontal location of 2000 km on the figure yields results in contradiction with our simple theoretical models; the precipitable water vapor anomaly is positive while the midtropospheric temperature anomaly is negative, both of which should produce a positive precipitation anomaly, yet the precipitation anomaly is zero at this point in the wave phase. One speculation as to why this is involves the vertical structure of the moisture anomaly; at low levels it is negative, even though the column integral is positive (Fig. 7). Such structure cannot be accounted for in models with a single vertical mode. Alternatively, we can look around 3500 km, where the temperature anomaly vanishes but the precipitable water vapor anomaly is around 0.5 mm. Using this and the precipitation anomaly gives a moisture time scale on the order of 0.2 d, much shorter than the estimate obtained from our stationary mode. However, again in this case the more complex vertical structure of the moisture field, with most of the anomaly at low levels, and the apparent disagreement at 2000 km weakens our confidence in the comparison.

6. Conclusions

Starting from a basic state of approximate radiative–convective equilibrium, we forced convectively coupled waves in the MM5 by imposing a heating with a traveling wave form and a maximum amplitude of 10 K d^{-1} for one day, then turning that heating off and allowing the induced wave to evolve freely for seven additional days. In all simulations, the waves decay initially by moist convective damping, but in two particular cases weakly damped or neutrally stable waves with very persistent, coherent "modal" structures emerge after this initial decay, and evolve with little change for the last several days of the simulations.

One of these waves is a convectively coupled gravity wave. Qualitatively, its structure is similar to those described by QE theory, but the interaction between convection and gravity wave dynamics is much weaker than predicted by ENB. Despite having essentially the vertical structure of the gravest baroclinic mode, its phase speed is faster than the simplest SQE theory (CAPE and relative humidity both constant with wave phase) predicts. The interaction between convection and the wave is weaker than that theory presumes, and as a result the diabatic heating is substantially smaller than the adiabatic cooling in the wave. This mode is destabilized by the evaporation–wind feedback, though not to the point of being actually unstable. Our attempt to use this wave to calibrate the convective time scales appearing in simple analytical theories such as ENB and Fuchs and Raymond (2002) leads to inconsistent results, perhaps because the moisture field has a more complex structure than such theories have assumed.

The other wave is stationary with respect to the mean flow and has a large signature in the moisture field. It resembles the stationary moisture anomalies simulated by Tompkins (2001) and the stationary moisture

waves appearing in the theoretical studies of Sobel et al. (2001) and Fuchs and Raymond (2002). The latter of those two studies predicted a mode essentially identical to that of Sobel et al. (2001) at high wavenumber, but a much more strongly damped mode at low wavenumber, with the cutoff wavenumber between these two regimes determined by uncertain parameters. Our simulated stationary mode, with a wavelength of 4500 km, suggests a "convective moisture time scale" on the order of 2.5 d, and has a decay time considerably longer than that. With such a long decay time, this mode resembles the high-wavenumber regime of Fuchs and Raymond (2001), and is also consistent with the mode which Sobel et al. (2001) obtained by applying the WTG approximation to the nonrotating, linearized QTCM equations.

All our results must be viewed subject to the caveats that they rely on a particular convective parameterization, and that they omit cloud–radiative feedbacks. The latter may significantly modify the modes' behavior; for example, Lee et al. (2001) found that cloud–radiative feedbacks could provide the primary driving mechanism for a mode otherwise similar to our stationary moisture mode in a general circulation model. Our view is that the simulations described here are nonetheless useful in that they allow explicit comparison between theoretical predictions and a model which is well known, widely used, and incorporates much more complexity and many fewer assumptions than the theories do. A logical, albeit computationally expensive, next step is to repeat similar experiments with cloud-resolving models.

7. Acknowledgements

This work was supported by NSF grant ATM-0096195 and NASA grant NAGS5-10624. Hui Su provided technical assistance with the MM5 in the very early phases of this work. Marc Michelsen's expert system management, and computational troubleshooting on our behalf specifically, were helpful throughout the project.

8. Appendix: Dry and moist phase speeds

To quantify the predictions of quasi-equilibrium theory in the simplest way, we make use of the QTCM equations (Neelin, 1997; Neelin and Zeng, 2000). In these equations, temperature and moisture perturbations have fixed vertical profiles:

$$T(x, y, p, t) = T_{ref}(p) + a(p)T_1(x, y, t) \tag{6}$$

$$q(x, y, p, t) = q_{ref} + b(p)q_1(x, y, t), \tag{7}$$

where T_{ref} and q_{ref} are reference profiles, not assumed to be solutions to any particular equations. T and q incorporate the heat capacity of dry air and latent heat of vaporization of water, so that both are in units of J kg^{-1}. Here we consider the linearized QTCM temperature and moisture equations in two dimensions (x and p), with perturbations in radiative heating and surface fluxes neglected:

$$\hat{a}\partial_t T_1 + M_s\partial_x u_1 = \hat{Q}_c \tag{8}$$

$$\hat{a}\partial_t q_1 - M_q\partial_x u_1 = -\hat{Q}_c. \tag{9}$$

Q_c is the convective heating, or equivalently precipitation, u_1 is the baroclinic horizontal (x) velocity, M_S is the dry static stability, and M_q the gross moisture stratification (see the above-cited original papers for further details). Hats (ˆ) represent averages in pressure through the depth of the troposphere.

If a and b are chosen to mimic changes following perturbations to a moist adiabat with a specified, fixed profile of relative humidity, one finds $\hat{a} \approx 0.4-0.5$ and $\hat{a} + \hat{b} \approx 0.9$. We add eqs. (8) and (9) and assume SQE, which in this system is expressed as $q_1 = T_1$, to obtain the moist static energy equation for convectively-coupled motions:

$$\partial_t h_1 + M\nabla \cdot \mathbf{v}_1 = 0$$

where $h_1 = (\hat{a} + \hat{b})T_1$, and $M = M_S - M_q$ is the gross moist stability.

On the other hand, dry dynamics alone ($Q_c = 0$) would give the corresponding dry static energy equation:

$$\hat{a}\partial_t T_1 + M_s\nabla \cdot \mathbf{v}_1 = 0.$$

The linearized QTCM momentum equation is

$$\partial_t u_1 = -\kappa\partial_x T_1,$$

where $\kappa = R/c_p$, the ratio of the gas constant of air to its heat capacity. We can put this together with the moist equation to get a wave equation with squared moist phase speed:

$$c_m^2 = \kappa M/(\hat{a} + \hat{b}).$$

The corresponding dry phase speed obeys:

$$c_d^2 = \kappa M_s/\hat{a}.$$

The ratio is

$$\frac{c_m^2}{c_d^2} = \frac{M}{M_s}\frac{\hat{a}}{\hat{a}+\hat{b}}.$$

The factor $\hat{a}/(\hat{a}+\hat{b})$ is roughly 0.5, which for $M/M_S = 0.35$ (as in the case of our fast mode), yields an expected phase speed about 30% of the dry one, or around 15 m s^{-1}, half of what occurs in the simulation.

However, in our fast wave, q_1 is quite small due to the compensation of RH and temperature between the cold and warm fast wave phases, so in fact $h_1 \approx \hat{a}T_1$, or equivalently we can take $\partial_t q_1 \approx 0$ in the above argument, as opposed to assuming SQE ($q_1 = T_1$). Doing this removes the factor $\hat{a}/(\hat{a}+\hat{b})$ and brings the phase speed into agreement with the simulations.

REFERENCES

Arakawa, A. and Schubert, W. H., 1974. Interaction of a cumulus cloud ensemble with the large-scale environment., *J. Atmos. Sci.* **31**, 674–701.

Betts, A. K. 1986. A new convective adjustment scheme. Part I: Observational and theoretical basis. *Q. J. R. Meteorol. Soc.* **112**, 677–691.

Betts, A. K. and Miller, M. J. 1986. A new convective adjustment scheme. Part II: Single column tests using Gate wave, BOMEX, ATEX and arctic air-mass data sets. *Q. J. R. Meteorol. Soc.* **112**, 693–709.

Blackadar, A. K. 1976. Modeling the nocturnal boundary layer. *Preprints, Third Symposium on Atmospheric Turbulence, Diffusion, and Air Quality*, Raleigh, Am. Meteorol. Soc. 46–49.

Blackadar, A. K. 1978. Modeling pollutant transfer during daytime convection. *Preprints, Fourth Symposium on Atmospheric Turbulence, Diffusion, and Air Quality*, Reno, Am. Meteorol. Soc. 443–447.

Cohen, C. and Frank, W. M. 1987. Simulation of tropical convective systems. Part II: Simulations of moving cloud lines. *J. Atmos. Sci.* **44**, 3800–3820.

Dudhia, J. 1989. Numerical study of convection observed during the winter monsoon experiment using a mesoscale, two-dimensional model. *J. Atmos. Sci.* **46**, 3077–3107.

Emanuel, K. A. 1987. An air–sea interaction model of intraseasonal variations in the tropics. *J. Atmos. Sci.* **44**, 2324–2340.

Emanuel, K. A., Neelin, J. D. and Bretherton, C. S. 1994. On large-scale circulations in convecting atmospheres. *Q. J. R. Meteorool. Soc.* **120**, 1111–1143.

Frank, W. M. 1993. A hybrid parameterization with multiple closures. *The representation of cumulus convection in numerical models* (eds. K. A. Emanuel and D. J. Raymond). American Meteorological Society, Boston, 246 pp.

Frank, W. M. and Cohen, C. 1987. Simulation of tropical convective systems. Part I: A cumulus parameterization. *J. Atmos. Sci.* **44**, 3787–3799.

Fritsch, J. M. and Chappell, C. F. 1980. Numerical prediction of convectively driven mesoscale pressure systems. Part I: Convective parameterization. *J. Atmos. Sci.* **37**, 1722–1733.

Fritsch, J. M. and Kain, J. S. 1993. Convective parameterization for mesoscale models: the Fritsch–Chappell scheme. *The representation of cumulus convection in numerical models* (eds. K. A. Emanuel and D. J. Raymond). American Meteorological Society, Boston, 246 pp.

Fuchs, Z. and Raymond, D. J. 2002. On the large-scale modes of a moist, nonrotating atmosphere. *J. Atmos. Sci.* **59**, 1669–1679.

Grell, G., Dudhia, J. and Stauffer, D. R. 1994. A description of the fifth-generation Penn State/NCAR mesoscale model (MM5). NCAR Technical Note, NCAR/TN-398+STR, 138 pp.

Heymsfield, A. J. and Donner, L. J., 1990. A scheme for parameterizing ice-cloud water content in general circulation models. *J. Atmos. Sci.* **47**, 1865–1877.

Kain, J. S. and Fritsch, J. M. 1990. A one-dimensional entraining/detraining plume model and its application in convective parameterization. *J. Atmos. Sci.* **47**, 2784–2802.

Kain, J. S. and Fritsch, J. M. 1993. Convective parameterization for mesoscale models: the Kain–Fritsch scheme. *The representation of cumulus convection in numerical models* (eds. K. A. Emanuel and D. J. Raymond). American Meteorological Society, Boston, 246 pp.

Kain, J. S. and Fritsch, J. M. 1998. Multiscale convective overturning in mesoscale convective systems: reconciling observations, simulations, and theory. *J. Fluid. Mech.* **126**, 2254–2273.

Klemp, J. B. and Durran, D. R. 1983. An upper boundary condition permitting internal gravity wave radiation in numerical mesoscale models. *Mon. Wea. Rev.* **111**, 430–444.

Lee, M.-I., Kang, I.-S., Kim, J.-K. and Mapes, B. E. 2001. Influence of cloud–radiation interaction on simulating tropical intraseasonal oscillation with an atmospheric general circulation model. *J. Geophys. Res.* **106**, 14219–14233.

Molinari, J. 1993. An overview of cumulus parameterization in mesoscale models. *The representation of cumulus convection in numerical models* (eds. K. A. Emanuel and D. J. Raymond). American Meteorological Society, Boston, 246 pp.

Molinari, J. and Dudek, M. 1992. Parameterization of convective precipitation in mesoscale numerical models: a critical review., *Mon. Wea. Rev.* **104**, 326–344.

Neelin, J. D. 1997. Implications of convective quasi-equilibrium for the large-scale flow. *The physics and parameterization of moist atmospheric convection* (ed R. K. Smith). Kluwer, Dardrecht, 413–446.

Neelin, J. D. and Held, I. M. 1987. Modeling tropical convergence based on the moist static energy budget. *Mon. Wea. Rev.* **115**, 3–12.

Neelin, J. D., Held, I. M. and Cook, K. H. 1987. Evaporation–wind feedback and low frequency variability in the tropical atmosphere. *J. Atmos. Sci.* **44**, 2341–2348.

Neelin, J. D. and Yu, J.-Y., 1994. Modes of tropical variability under convective adjustment and the Madden-Julian oscillation. Part I: Analytical theory. *J. Atmos. Sci.* **51**, 1876–1894.

Neelin, J. D. and Zeng, N. 2000. The first quasi-equilibrium tropical circulation model-formulation. *J. Atmos. Sci.* **57**, 1741–1766.

Raymond, D. J. 2000. The Hadley circulation as a radiative–convective instability. *J. Atmos. Sci.* **57**, 1286–1297.

Sobel, A. H., Nilsson, J. and Polvani, L. M. 2001. The weak temperature gradient approximation and balanced tropical moisture waves. *J. Atmos. Sci.* **58**, 3650–3665.

Su, H., Bretherton, C. S. and Chen, S. S. 2000. 'Self-aggregation' and 'large-scale control' of tropical deep convection: a modeling study. *J. Atmos. Sci.* **57**, 1797–1816.

Tompkins, A. M. 2001. Organization of tropical convection in low vertical wind shears: the role of water vapor. *J. Atmos. Sci.* **58**, 529–545.

Wheeler, M. and Kiladis, G. N. 1999. Convectively coupled equatorial waves: analysis of clouds and temperature in the wavenumber–frequency domain. *J. Atmos. Sci.* **56**, 374–399.

Yu, J.-Y., Chou, C. and Neelin, J. D. 1998. Estimating the gross moist stability of the tropical atmosphere. *J. Atmos. Sci.* **55**, 1354–1372.

Zeng, N., Neelin, J. D. and Chou, C. 2000. Quasi-equilibrium tropical circulation model—implementation and simulation. *J. Atmos. Sci.* **57**, 1767–1796.

Zhang, D. and Anthes, R. A. 1982. High-resolution model of the planetary boundary layer: sensitivity tests and comparisons with SESAME-79 data. *J. Appl. Meteorol* **21**, 1594–1609.